American Mineralogist, Volume 91, pages 1293–1299, 2006

Stacking structures in pyrophyllite revealed by high-resolution transmission electron microscopy (HRTEM)

TOSHIHIRO KOGURE,[1,2,*] MAYUMI JIGE,[3] JUN KAMEDA,[1] AKIHIKO YAMAGISHI,[1,2] RITSURO MIYAWAKI,[4] AND RYUJI KITAGAWA[3]

[1]Department of Earth and Planetary Science, Graduate School of Science, The University of Tokyo, 7-3-1 Hongo, Bunkyo-ku, Tokyo, 113-0033, Japan
[2]CREST, Japan Science and Technology Corporation, Honcho 4-1-8, Kawaguchi, Saitama 332-0012, Japan
[3]Department of Earth and Planetary Sciences, Faculty of Sciences, Hiroshima University, 1-3-1 Kagamiyama, Higashi-Hiroshima, 739-8526, Japan
[4]Department of Geology, The National Science Museum, 3-23-1 Hyakunin-cho, Shinjuku-ku, Tokyo 169-0073, Japan

ABSTRACT

Stacking structures in pyrophyllite, $Al_2Si_4O_{10}(OH)_2$, were investigated mainly by using high-resolution transmission electron microscopy (HRTEM). The specimens examined were large lath-shaped crystals (Berosovska, Urals, Russia) and massive aggregates of fine platy crystals (Nohwa, southwest Korea). Both specimens showed powder X-ray diffraction (XRD) patterns similar to those reported previously as the 2*M* polytype. The common stacking sequence in the two specimens is not monoclinic with two-layer periodicity as previously reported, but a uniform orientation of the 2:1 layers and near complete disorder of two alternative directions of interlayer displacement, i.e., lateral displacement between the two tetrahedral sheets across an interlayer region. The directions of interlayer displacement are about $\pm 2\pi/3$ from that of the intralayer shift (lateral displacement between the two tetrahedral sheets within a 2:1 layer). Simulation of powder XRD patterns by this stacking model closely approximates the experimental pattern. Elongation of the lath-shaped Berosovska crystals corresponds to the direction of the intralayer shift, as seen in illite-1*M*.

2:1 layers with different orientations, and interlayer displacement almost parallel to the intralayer shift, were occasionally observed as stacking faults. Such disorder occurs more frequently in the massive Nohwa specimen than in the Berosovska specimen. Sub-micrometer domains of the 2*M* stacking sequence with regular alternation of the two directions of interlayer displacement were found in the Nohwa specimen.

Keywords: Crystal structure, pyrophyllite, electron microscopy, order-disorder, XRD data

INTRODUCTION

Pyrophyllite and talc are unique 2:1 phyllosilicate minerals because there is a neutral layer charge, which requires a vacant interlayer region. Their stacking sequences may be complicated owing to the absence of interlayer cations that interlock adjacent 2:1 layers. Zvyagin et al. (1969) suggested from electron-diffraction analyses that lateral displacement between the two tetrahedral sheets across the interlayer of pyrophyllite and talc can be almost $\pm \boldsymbol{a}_i/3$ (i = 1, 2, or 3) where $\pm \boldsymbol{a}_i$ are the vectors connecting the centers of adjacent hexagonal rings in a tetrahedral sheet. They defined the displacement with the symbol "τ", which is referred to as "interlayer displacement" in the present study. The origin of interlayer displacement results from the minimization of repulsive forces between the two tetrahedral sheets across the interlayer (Zvyagin et al. 1969). Ďurovič and Weiss (1983) showed that pyrophyllite can potentially adopt 30 non-congruent (22 non-equivalent) MDO (Maximum Degree of Order, named also "standard," "regular," etc. by other researchers) polytypes by the choice of layer orientation, the direction of interlayer displacement, and the position of the octahedral vacancy.

Two ordered polytypes were reported in pyrophyllite. Gruner (1934) and Hendricks (1938) proposed a monoclinic unit cell with two-layer periodicity. Zvyagin et al. (1969) reported that natural pyrophyllite is two-layer monoclinic and synthetic pyrophyllite adopts a one-layer triclinic cell. Using their symbolism, the stacking sequence of the monoclinic polytype was reported as $\sigma_3\tau_5\sigma_3\tau_1\sigma_3$, while that of the triclinic polytype was reported as $\sigma_2\tau_4\sigma_2$. Brindley and Wardle (1970) measured powder X-ray diffraction (XRD) patterns of many natural pyrophyllite specimens that can be indexed by one-layer triclinic (pyrophyllite-1*A*, originally -1*Tc*) and two-layer monoclinic (pyrophyllite-2*M*) cells. Eberl (1979) performed synthetic experiments and reported that 1*A* forms at higher temperatures than 2*M*.

The crystal structure of pyrophyllite-1*A* was precisely determined by Wardle and Brindley (1972) from powder XRD and later by Lee and Guggenheim (1981) using a single crystal. The stacking sequence determined for pyrophyllite-1*A* agrees with that proposed by Zvyagin et al. (1969). The intralayer shift, or lateral displacement between the lower and upper tetrahedral sheets in a 2:1 layer with a shift of $a/3$, is along $[\bar{1}\bar{1}0]$. The interlayer displacement is close to but deviates by about 3° from $[\bar{1}10]$, which is about 7% shorter than $a/3$ (Lee and Guggenheim 1981) and results in the α angle of about 91.2°.

In contrast, the structure of pyrophyllite-2*M* has not been

* E-mail: kogure@eps.s.u-tokyo.ac.jp

0003-004X/06/0809–1293$05.00/DOI: 10.2138/am.2006.1997

clearly settled. First, there seems to be no strong evidence for two-layer periodicity in the powder XRD pattern of pyrophyllite-2*M* as described in Brindley and Wardle (1970). Furthermore, it seems unlikely that 2*M* forms at lower temperatures than 1*A* (Eberl 1979), which is different from the relationship between 1*M* and $2M_1$ polytypes in muscovite (Evans and Guggenheim 1988, p. 232).

We investigated stacking structures in diverse phyllosilicates by using high-resolution transmission electron microscopy (HRTEM). To our knowledge, no HRTEM work elucidating the stacking sequences in pyrophyllite has been reported. The present study is probably the first to directly image the stacking sequence in pyrophyllite, which reveals the true structure of pyrophyllite-2*M* and various stacking structures in the mineral.

Samples and methods

Two pyrophyllite specimens with different morphologies were examined in this study. One consists of green-colored, large, lath-shaped crystals from Berozovska, Urals, Russia (Brindley and Wardle 1970). This specimen appears as radial aggregates in veins (Fig. 1a). The length of the crystals is up to 3 cm. Another specimen consists of grayish, massive aggregates of fine platy crystals (Fig. 1b) from Nohwa, southeast Korea (Kitagawa et al. 1999). Electron microprobe analyses of the specimens were performed on a JEOL JXA-8200R electron microprobe analyzer. Accelerating voltage and specimen current were kept at 15 kV and 12 nA on a Faraday cup, respectively. The beam diameter was 2 µm. Wollastonite (for Si), rutile (Ti), corundum (Al), hematite (Fe), MnO (Mn), Cr_2O_3 (Cr), periclase (Mg), wollastonite (Ca), jadeite (Na), and $KTiPO_5$ (K) were used as standards. The Bence and Albee (1968) method was employed for matrix corrections and the oxidation state of Fe was assumed divalent. The result is shown in Table 1. Powder XRD patterns were collected using a Rigaku RINT-Ultima+ diffractometer with Cu*K*α radiation, a graphite monochromator, a 0.3 mm receiving slit, and 1° divergence and anti-scatter slits. A continuous scan rate of 1° (2θ) min^{-1} was adopted.

Specimens for TEM examination were prepared by using a method similar to that described by Kogure (2002). Crushed Berozovska crystals were embedded with epoxy resin between two glass slides. After hardening, the glass slides were cut using a diamond wheel to laths of about 1 mm thickness. The laths were thinned to about 50 µm by mechanical grinding and finished by argon ion milling. A petrographic thin section was made of the massive Nohwa specimen. Disks of about 3 mm in diameter were obtained from the section and thinned to be electron-transparent by argon ion milling. HRTEM examination was performed at 200 kV using a JEOL JEM-2010 with a nominal point resolution of 2.0 Å (C_s = 0.5 mm). Degradation in pyrophyllite by electron radiation is rapid but not as serious as in kaolin minerals (Kogure and Inoue 2005). Radiation damage is also dependent on stacking sequences as described below. Therefore, generally only one exposure was possible to obtain HRTEM images with magnification of ×400 000 or ×500 000 on film. Some successful images as recorded on films were digitized using a CCD camera for image processing. Noise from amorphous materials on the specimen surfaces was removed using the rotational filtering technique (Kilaas 1998) implemented with Gatan DigitalMicrograph version 2.5 (with respect to the performance of the filtering, see Kogure and Banfield 1998). Multi-slice image simulation was performed using MacTempas (Total Resolution Co.).

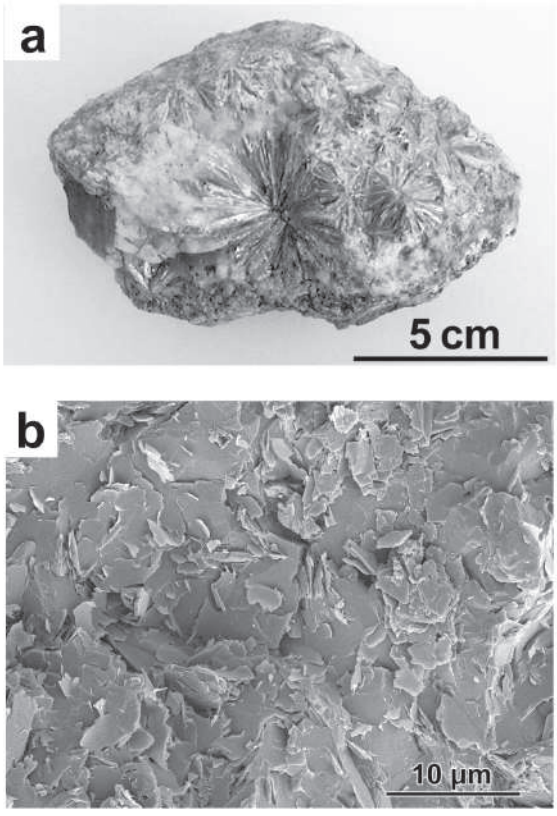

Figure 1. (**a**) Radial aggregates of lath-shaped pyrophyllite crystals from Berozovska, Urals, Russia. (**b**) SEM micrograph of a fracture surface of massive pyrophyllite from Nohwa, southeast Korea.

Results and discussion

General stacking sequence in pyrophyllite

Figure 2 shows a powder XRD pattern from each specimen. Finely powdered specimens were side-loaded in a cavity on a glass slide to avoid preferred orientation (Brindley and Wardle 1970). Despite the different macroscopic appearances of the two specimens, their XRD patterns are similar (Berozovska specimen shows slight preferred orientation). Small peaks in the pattern of the Berozovska specimen are from sudoite (Jige et al. 2003). The two broad peaks around d = 4.42 Å (arrow "A") and 4.18 Å ("B") are characteristic, and the patterns are similar to that interpreted as pyrophyllite-2*M* by Brindley and Wardle (1970) and Eberl (1979). However, neither study described the rationale for assigning a two-layer periodicity and the origin of the broadening of the peaks.

From these XRD and selected area electron diffraction (SAED) patterns along the ***b***-axis (not shown), it is confirmed that the general stacking sequence for both specimens belongs to subfamily A (Ďurovič and Weiss 1983). In other words, the angles between the directions of any shifts (intralayer shift and interlayer displacement) in the stacking sequence are either 0 or ±2π/3. Hence, the stacking sequence of the specimens can be analyzed from an HRTEM image along only one of the $\pm\boldsymbol{a}_i$ vectors (Kogure 2002). Simulated HRTEM images for pyrophyllite-1*A*, using atomic coordinates reported by Lee and Guggenheim (1981) are shown in Figure 3. Parameters for the simulation are given

Table 1. Chemical analysis (wt%) of the pyrophyllite specimens

	Berozovska	Nohwa
SiO_2	67.2	67.6
TiO_2	–	–
Al_2O_3	27.9	28.9
FeO	0.1	0.3
MnO	–	–
Cr_2O_3	0.1	–
MgO	–	–
CaO	–	–
Na_2O	–	0.2
K_2O	–	0.1
Total	95.3	97.0

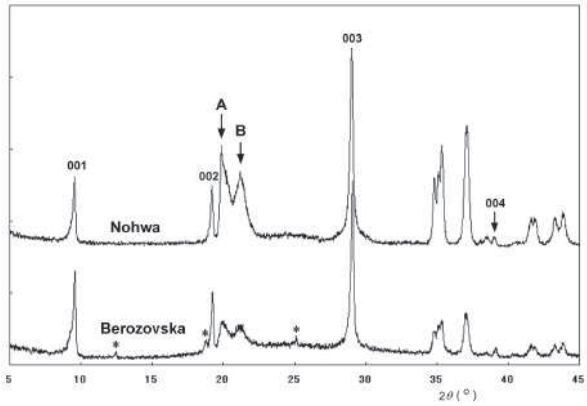

FIGURE 2. Powder XRD patterns from the Berozovska and Nohwa specimens. The basal reflections are indexed, assuming one-layer periodicity. The small peaks with asterisk in the pattern of Berozovska specimen are from sudoite.

in the caption. Contrast at the tetrahedral or dioctahedral sheets in a 2:1 layer consist of dark spots that correspond to a pair of Si tetrahedra or Al octahedra, separated by $b/2$ (= 4.5 Å) in the sheets. When the beam direction is parallel or anti-parallel to the intralayer shift (±[110] in case of pyrophyllite-1*A*), these three spots (Fig. 3) in a 2:1 layer are aligned vertically. Dark spots for the two tetrahedral sheets across the interlayer are shifted if observed along ±[110] or ±[100] but not shifted if observed along ±[$\bar{1}$10], depending on the relationship between the beam direction and that of interlayer displacement.

Figure 4 shows an experimental HRTEM image in the Berozovska specimen. By comparing this image with those in Figure 3, it is easily recognized that the intralayer shift of all 2:1 layers is uniform, parallel (or anti-parallel) to the beam direction. However, the shift directions between adjacent 2:1 layers are generally disordered with alternative positions to the left or right, indicating that the direction of interlayer displacement is about $+2\pi/3$ or $-2\pi/3$ from that of the intralayer shift, with the assumption that the stacking sequence belongs to subfamily A.

To make the correspondence between this stacking sequence and the powder XRD patterns, a simulation of the diffraction pattern using DIFFaX (Treacy et al. 1991) was performed. In the simulation, two kinds of layers were used. Layer 1 is a 2:1 layer, which is positioned on the preceding layer with the direction of interlayer displacement of $+2\pi/3$. Layer 2 is an identical 2:1 layer but positioned on the preceding layer with the direction of interlayer displacement of $-2\pi/3$. The stacking sequence is expressed by a 2×2 matrix (α_{ij}) where α_{ij} is the probability for layer *j* positioned on layer *i*. This matrix can be expressed simply by a parameter "*p*" as

$$\alpha_{11} = p, \qquad \alpha_{12} = 1 - p$$
$$\alpha_{21} = 1 - p, \qquad \alpha_{22} = p$$

If $p = 1$, the direction of interlayer displacement is the same ($+2\pi/3$ or $-2\pi/3$) at each interlayer regions, which describes the 1*A* polytype. If $p = 0$, the stacking sequence is 2*M* as suggested by Zvyagin et al. (1969) ($\sigma_3\tau_5\sigma_3\tau_1\sigma_3$) in which the direction of interlayer displacement is the regular alternation of $+2\pi/3$ and $-2\pi/3$. If $p = 0.5$, the stacking is perfectly random with $+2\pi/3$ or $-2\pi/3$. If p is between 0 and 0.5, there is a tendency to form 2*M* rather than 1*A*, and this is reversed with $0.5 < p < 1$. Figure 5 shows the simulated powder XRD patterns with various p values. The pattern for 1*A* ($p = 1$) is identical with that reported by Blindley and Wardle (1970) and the pattern for 2*M* ($p = 0$) is comparable to that calculated by Weiss and Ďurovič (1984). The pattern with $p = 0.5$ reproduces well the two broad peaks observed in the experimental XRD (Fig. 2). As noted above, this stacking sequence (termed $1A_d$ in the present study in parallel with $1M_d$ for the disordered mica belonging to subfamily A) indicates perfect disorder of the two directions. Figure 6 represents calculated diffraction patterns by DIFFaX. The broad peak at the lower angle in the powder XRD ("A" in Fig. 2) is generated by the intense band marked "A" on the $hk = 1\bar{1}$ row in Figure 6c. Another broad peak at the higher angle ("B" in Fig. 2) corresponds to the bands marked "B" on the 11 and 02 rows in Figures 6a and 6b. Figure 6d shows the

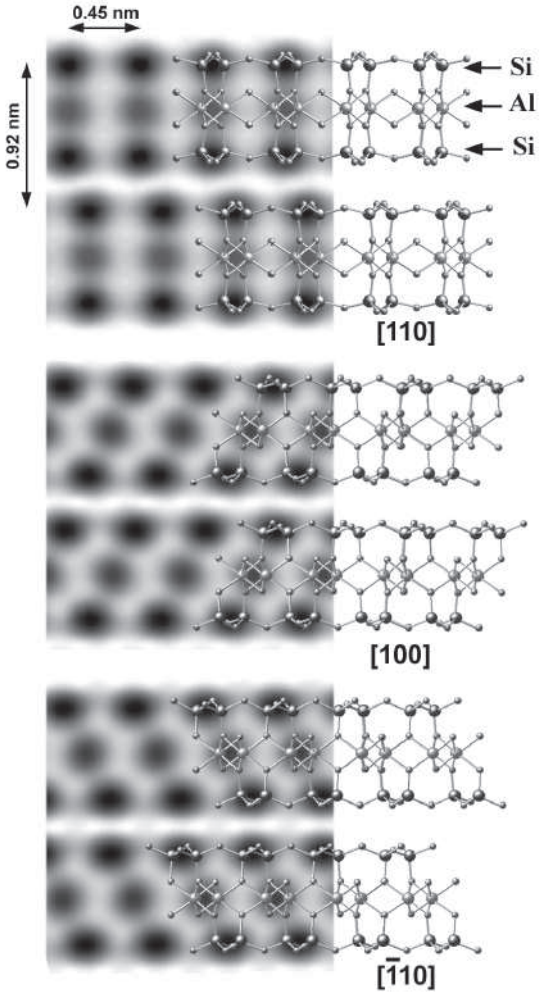

FIGURE 3. Crystal structure and multi-slice computer simulation for the HRTEM contrasts of pyrophyllite-1*A* along three directions. The parameters for the simulation are as follows. Specimen thickness = 2.5 nm; Defocus = –40 nm; Acceleration voltage = 200 kV; Spherical aberration coefficient (C_s) = 0.5 mm; Spread of focus = 10 nm.

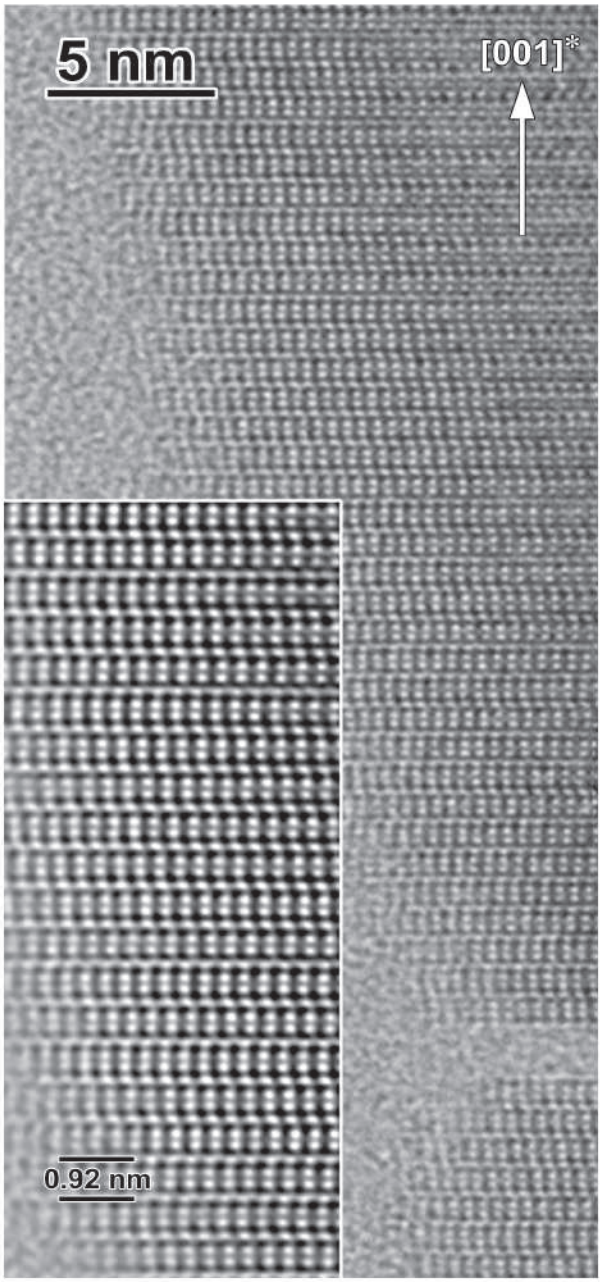

FIGURE 4. HRTEM photograph from the Berozovska specimen. The inset in the bottom-left is a filtered and magnified image from a portion of the photograph. Notice that the contrast for each 2:1 layer is uniform but the direction of shift between adjacent layers is near-perfectly disordered.

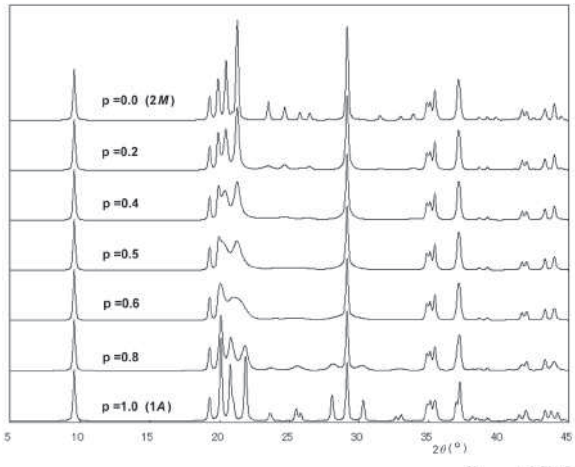

FIGURE 5. Simulated powder XRD patterns for various stacking sequences (see the text), using DIFFaX (Treacy et al. 1991). The atomic coordinates reported by Lee and Guggenheim (1981) were used for the calculation. In the calculation, a pseudo-Voigt function (the same ratio of Gauss and Lorentz functions) with a half-width of 0.2° was assumed for the peak profile.

experimental SAED pattern from the image in Figure 3, which corresponds to the simulated pattern in Figure 6c. Although the intensity distribution in the SAED pattern in Figure 6d is not a perfect match to the kinematically calculated pattern in Figure 6c, similar characteristics (i.e., the $\bar{1}1$ row is heavily streaked but the $2\bar{2}$ row is not) are found in both patterns.

$1A_d$ is the dominant stacking sequence in both specimens because the powder XRD patterns in Figure 2 are explained by the sequence. This was also confirmed by TEM observations of many different views in both specimens. Brindley and Wardle (1970) investigated 16 pyrophyllite specimens from different localities by powder XRD and reported that "monoclinic" ($1A_d$ in reality) was the most abundant. The experimental result of Eberl (1979) that the "monoclinic" polytype forms at lower temperature than the triclinic now seems reasonable, because the transition from disordered stacking sequences to ordered sequences by elevating temperature is a common phenomenon for phyllosilicates (e.g., Hayes 1970; Beaufort et al. 1998).

The two directions of interlayer displacement in $1A_d$ must be closely related to the configuration of the basal oxygen plane in the 2:1 layer reported by Wardle and Brindley (1972), and Lee and Guggenheim (1981). Both works described a corrugation of basal oxygen atoms along [110] in pyrophyllite-1*A*, or along the direction of the intralayer shift, which is caused by the twist of the Si tetrahedra to form a large vacant site in the dioctahedral sheet. This corrugation breaks the trigonal symmetry although a pseudo-mirror plane parallel to the intralayer shift remains distinctive in the basal oxygen plane. The pseudo-mirror symmetry is the origin for the similar probability of the directions of interlayer displacement with $+2\pi/3$ or $-2\pi/3$ from that of the intralayer shift. In contrast, interlayer displacement with the same direction as that of the intralayer shift, or parallel to the corrugation, probably generates an unfavorable configuration of the two basal oxygen planes across the interlayer region. A similar situation for stacking was also reported in disordered kaolinite (Kogure and Inoue 2005).

Other stacking faults in pyrophyllite

Besides the disorder between the alternative directions for interlayer displacement, other kinds of stacking disorder were

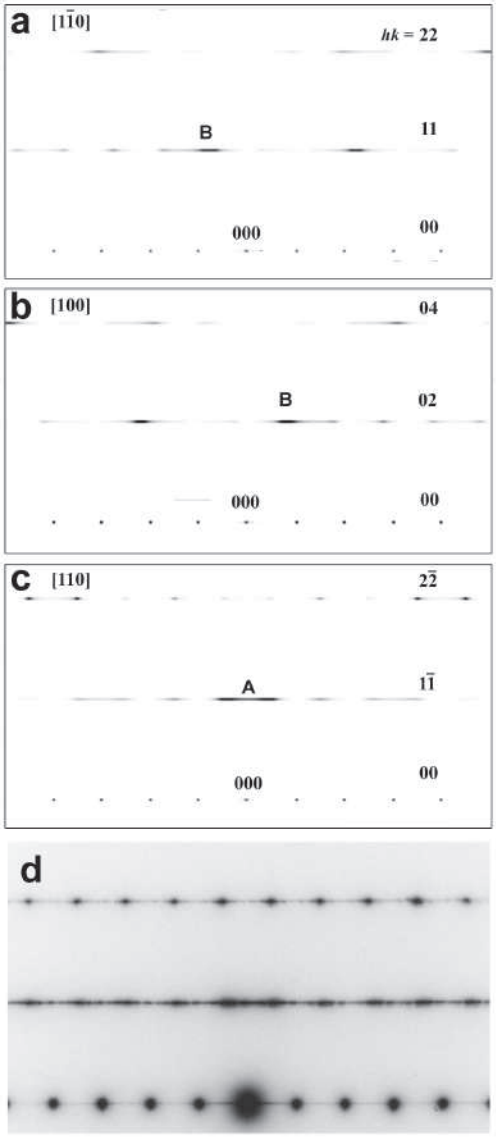

FIGURE 6. (**a**–**c**) Calculated diffraction patterns from $1A_d$ stacking sequence (p = 0.5 in Fig. 5), using DIFFaX. The intense band marked "A" on the $\bar{1}1$ row corresponds to the broad peak A in Figure 2, and those marked "B" on the 02 and 11 rows correspond to the peak B in Figure 2 (see the text for the detail). (**d**) Experimental SAED pattern from the image in Figure 4, which corresponds to the calculated pattern in **c**.

occasionally observed in the two specimens. Figure 7 is a HRTEM image from the Berozovska specimen, showing radiation damage roughly parallel to the (001) plane as indicated by the arrows. These damaged areas contain a 2:1 layer with a different direction of the intralayer shift, as shown in the magnified and filtered images to the right. Amorphization by radiation is very rapid around these layers with a different orientation, implying that such a layer rotation is energetically unfavorable in the pyrophyllite structure.

Disorder of layer orientation is more frequent in the massive Nohwa specimen than in the Berozovska specimen. Figure 8 shows a HRTEM image (the imaging condition was not optimized owing to rapid damage) from the Nohwa specimen, containing severe disorder of layer orientation. TEM specimens of the Berozovska pyrophyllite, which were prepared so that the elongated direction of the crystals were parallel to the electron beam, always showed HRTEM images like Figure 3, suggesting that the elongation is parallel to the direction of intralayer shift. Thus, the lath-shape of pyrophyllite probably results from an ordering of layer orientation, regardless of the order-disorder of the directions of interlayer displacement. This is similar to the fibrous morphology of illite-1*M* (Güven 1974). The massive Nohwa specimen does not show such an elongated crystal form (Fig. 1b). This may be related to greater disorder of the layer orientation in this specimen.

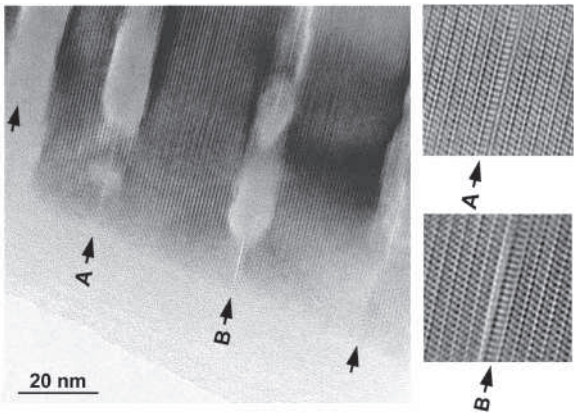

FIGURE 7. HRTEM image from the Berozovska specimen with radiation damage formed approximately parallel to the (001) plane, as indicated with the arrows. The right is magnified and filtered images of the damaged regions, showing existence of a layer with different orientation.

Another stacking disorder is interlayer displacement with a different direction from $\pm 2\pi/3$. Figure 9a shows a HRTEM image from the Berozovska specimen. The shift direction of the contrast at the interlayer region marked with the asterisk is unique from the others. This is interpreted as interlayer displacement with the same direction as that of intralayer shift. Similarly, interlayer displacement between two layers with different orientations does not have the $\pm 2\pi/3$ relation with both layers (Fig. 9b). In this figure, the contrasts of the two tetrahedral sheets across the interlayer are not shifted or only very slightly shifted at the interlayer regions, marked with arrows, indicating that the direction of interlayer displacement at these regions is nearly parallel or anti-parallel to the beam. Therefore, the interlayer displacement is also parallel or anti-parallel to the intralayer shift in the layers with contrast like the vertical bar (the contrast for [110] in Fig. 2) in Figure 9b. Because the corrugations in the two basal-oxygen planes across the interlayer are not parallel owing to layer rotation, energetically favorable interlayer displacement (its direction and amount) must not be the same as that reported in pyrophyllite-1*A*. It is obvious that a HRTEM image along only one direction is not sufficient but another image along a different

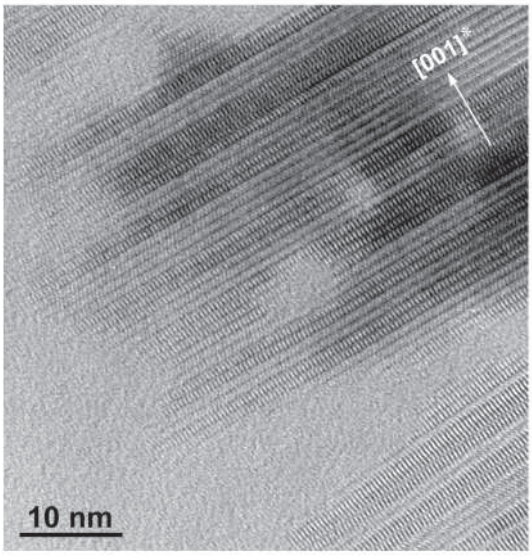

FIGURE 8. HRTEM image from the Nohwa specimen, showing disorder of layer orientations.

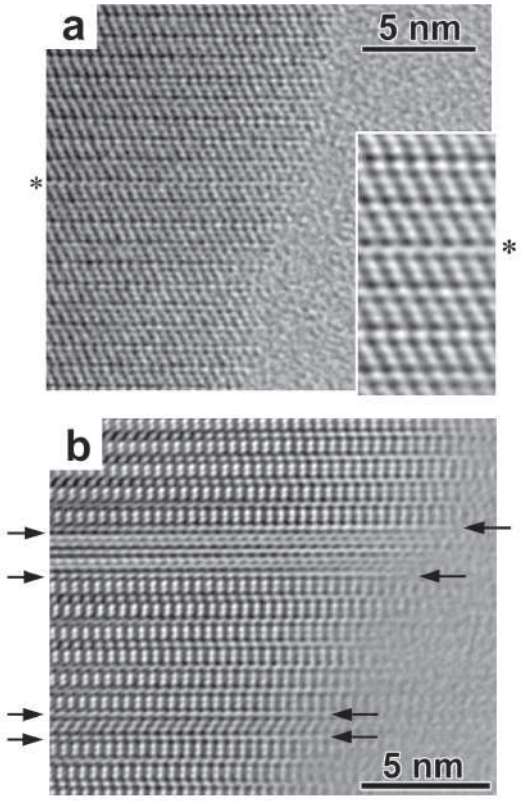

FIGURE 9. (**a**) High-resolution image from the Berozovska specimen and its magnified and filtered image in the right. At the interlayer region with asterisk the upper tetrahedral sheet is shifted to right from the lower sheet, whereas they are not shifted or shifted to left at the other interlayer regions. (**b**) Filtered HRTEM image from the Nohwa specimen containing layers with different layer orientations. Two tetrahedral sheets across the interlayer regions (arrowed) between adjacent layers with different orientations are not or weakly shifted (see the text).

direction is required to determine quantitatively the direction and amount of the interlayer displacement at these interlayer regions (Kogure and Nespolo 2001). Perfect imaging with sufficiently small misorientation and astigmatism is also required.

Possibility of the two-layer polytype

As noted above, the powder XRD pattern previously interpreted as monoclinic (2*M*) corresponds to disordered stacking with two alternative interlayer displacement directions. However, Hendricks (1938) reported a two-layer monoclinic unit cell using Weissenberg photographs from single crystals. Zvyagin et al. (1969) also proposed a two-layer polytype ($\sigma_3\tau_5\sigma_3\tau_1\sigma_3$) from oblique texture electron diffraction. It is possible that these results involve a misinterpretation related to twinned pyrophyllite-1*A* (Rayner and Brown 1973).

Domains with two-layer periodicity were found in the Nohwa specimen. Figure 10 shows a SAED pattern and an HRTEM image, showing two-layer periodicity. Although the contrast of the image is reversed by over-focusing, this image is interpreted as a stacking sequence with uniform layer orientation and alternation of the two directions ($+2\pi/3$ and $-2\pi/3$) of interlayer displacement, as suggested by Zvyagin et al. (1969). The size of the domain in which regular two-layer periodicity is formed is approximately 100 nm. It is not certain but this stacking sequence is probably an accidental product of spiral crystal growth (Kitagawa 1992) rather than an indication that the 2*M* stacking sequence is energetically more favorable than 1*A*, because the

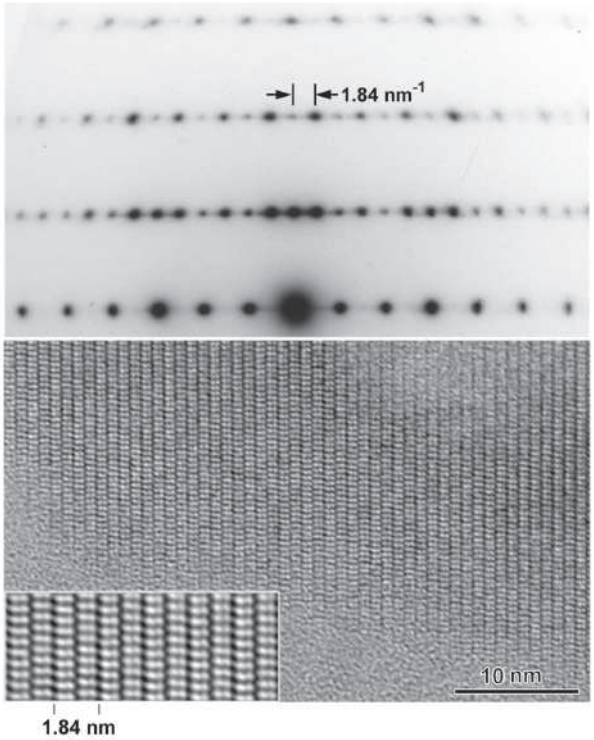

FIGURE 10. HRTEM image and corresponding SAED pattern from the domain with two-layer periodicity, found in the Nohwa specimen. The inset in the bottom-left is a filtered image of a portion of the raw image. Notice that the contrast is reversed due to over-focusing.

Nohwa specimen also contains frequently unfavorable stacking sequences with layer rotation as shown in Figure 8.

ACKNOWLEDGMENTS

We thank S. Guggenheim (University of Illinois at Chicago) and V.A. Drits (Russian Academy of Sciences) for their valuable comments, M. Mellini and M. Krekeler for their reviews, and J. Feinberg (A.E.) for handling of the manuscript. We are also grateful to T. Takeshige (University of Tokyo) for preparation of the TEM specimens. Transmission electron microscopy was performed in the Electron Microbeam Analysis Facility of Department of Earth and Planetary Science, University of Tokyo. This work was partly supported by a Grant-in-Aid no. 17340160 (Section B) by Japan Society for the Promotion of Science (JSPS).

REFERENCES CITED

Beaufort, D., Cassangnabere, A., Petit, S., Lanson, B., Berger, G., Lacharpagne, J.C., and Johansen, H. (1998) Kaolinite-to-dickite reaction in sandstone reservoirs. Clay Minerals, 33, 297–316.

Bence, A.E. and Albee, A.L. (1968) Empirical correction factors for the electron microanalysis of silicates and oxides. Journal of Geology, 76, 382–403.

Brindley, G.W. and Wardle, R. (1970) Monoclinic and triclinic forms of pyrophyllite and pyrophyllite anhydride. American Mineralogist, 55, 1259–1272.

Ďurovič, S. and Weiss, Z. (1983) Polytypism of pyrophyllite and talc. Part I OD interpretation and MDO polytypes. Silikáty, 27, 1–18.

Eberl, D. (1979) Synthesis of pyrophyllite polytypes and mixed layers. American Mineralogist, 64, 1091–1096.

Evans, B.W. and Guggenheim, S. (1988) Talc, pyrophyllite, and related minerals. In S.W. Bailey, Ed., Hydrous Phyllosilicates (exclusive of micas), 19, p. 225–294. Reviews in Mineralogy, Mineralogical Society of America, Chantilly, Virginia.

Gruner, J.W. (1934) The crystal structure of talc and pyrophyllite. Zeitschrift für Kristallographie, 88, 412–419.

Güven, N. (1974) Lath-shaped units in fine-grained micas and smectite. Clays and Clay Minerals, 22, 385–390.

Hayes, J.B. (1970) Polytypism of chlorite in sedimentary rocks. Clays and Clay Minerals, 18, 285–306.

Hendricks, S.B. (1938) The crystal structure of talc and pyrophyllite. Zeitschrift für Kristallographie, 99, 264–274.

Jige, M., Kitagawa, R., Zaykov, V.V., and Sinyakovskaya, I. (2003) Surface microtopography of sudoite. Clay Minerals, 38, 375–382.

Kilaas, R. (1998) Optical and near-optical filters in high-resolution electron microscopy. Journal of Microscopy, 190, 45–51.

Kitagawa, R. (1992) Surface microtopographies of pyrophyllite from the Shokozan area, Chugoku Province, southwest Japan. Clay Science, 8, 285–295.

Kitagawa, R., Nishido, H., Hwang, J.-Y., and Yang, P. (1999) Geochronological study of pyrophyllite deposits in East Asia. Resource Geology, 20, 123–128.

Kogure, T. (2002) Investigation of micas using advanced TEM. In A. Mottana, F.P. Sassi, J.B. Thompson, Jr., S. Guggenheim, Eds., Micas: Crystal Chemistry and Metamorphic Petrology, 46, p. 281–312. Reviews in Mineralogy and Geochemistry, Mineralogical Society of America, Chantilly, Virginia.

Kogure, T. and Banfield, J.F. (1998) Direct identification of the six polytypes of chlorite characterized by semi-random stacking. American Mineralogist, 83, 925–930.

Kogure, T. and Inoue, A. (2005) Determination of defect structures in kaolin minerals by High-Resolution Transmission Electron Microscopy (HRTEM). American Mineralogist, 90, 85–89.

Kogure, T. and Nespolo, M. (2001) Atomic structures of planar defects in oxybiotite. American Mineralogist, 86, 336–340.

Lee, J.H. and Guggenheim, S. (1981) Single crystal X-ray refinement of pyrophyllite-1*Tc*. American Mineralogist, 66, 350–357.

Rayner, J.H. and Brown, G. (1973) The crystal structure of talc. Clays and Clay Minerals, 21, 103–114.

Treacy, M.M.J., Newsam, J.M., and Deem, M.W. (1991) A general recursion method for calculating diffracted intensities from crystals containing planar faults. Proceedings of the Royal Society of London A, 433, 499–520.

Wardle, R. and Brindley, G.W. (1972) The crystal structure of pyrophyllite-1*Tc*, and of its dehydroxylate. American Mineralogist, 57, 732–750.

Weiss, Z. and Ďurovič, S. (1984) Polytypism of pyrophyllite and talc. Part II Classification and X-ray identification of MDO polytypes. Silikáty, 28, 289–309.

Zvyagin, B.B., Mishchenko, K.S., and Soboleva, S.V. (1969) Structure of pyrophyllite and talc in relation to the polytypes of mica-type minerals. Soviet Physics—Crystallography, 13, 511–515.

MANUSCRIPT RECEIVED JUNE 3, 2005
MANUSCRIPT ACCEPTED MARCH 28, 2006
MANUSCRIPT HANDLED BY JOSHUA FEINBERG